Hindawi Publishing Corporation
EURASIP Journal on Wireless Communications and Networking
Volume 2009, Article ID 806209, 12 pages
doi:10.1155/2009/806209

Research Article

Ultra-Wideband Channel Modeling for Intravehicle Environment

Weihong Niu,[1] Jia Li,[1] and Timothy Talty[2]

[1] *Department of Electrical and Computer Engineering, Oakland University, Rochester, MI 48309, USA*
[2] *ECI Laboratory, General Motors Research and Development Center, Warren, MI 48090, USA*

Correspondence should be addressed to Weihong Niu, wniu@oakland.edu

Received 7 May 2008; Revised 10 November 2008; Accepted 16 January 2009

Recommended by Weidong Xiang

With its fine immunity to multipath fading, ultra-wideband (UWB) is considered to be a potential technique in constructing intravehicle wireless sensor networks. In the UWB literature, extensive measuring and modeling work have been done for indoor or outdoor propagation, but very few measurements were performed in intravehicle environments. This paper reports our effort in measuring and modeling the UWB propagation channel in commercial vehicle environment. In our experiment, channel sounding is performed in time domain for two environments. In one environment, the transmitting and the receiving antennas are put beneath the chassis. In another environment, both antennas are located inside the engine compartment. It is observed that paths arrive in clusters in the latter environment but such clustering phenomenon does not exist in the former case. Different multipath models are used to describe the two different propagation channels. For the engine compartment environment, we describe the multipath propagation with the classical S-V model. And for the chassis environment, the channel impulse response is just represented as the sum of multiple paths. Observation reveals that the power delay profile (PDP) in this environment does not start with a sharp maximum but has a rising edge. A modified S-V PDP model is used to account for this rising edge. Based on the analysis of the measured data, channel model parameters are extracted for both environments.

1. Introduction

Electronic subsystems are essential components of modern vehicles. For the purpose of safety, comfort, and convenience, more and more sensors are being deployed in the new models of automotives to collect information such as temperature, speed, pressure, and so on. It is reported that the average number of sensors per vehicle already exceeds 27 in 2002 [1, 2]. Currently, sensors are connected to the electronic control unit (ECU) via cables for the transmission of collected data. As a result, the length of cables used for this purpose can add up to as many as 1000 meters [3]. In addition, the wire harness contributes at least 50 kg to the weight of a vehicle [3]. This not only greatly increases the complication of vehicle design but also negatively affects the cost, fuel economy, and environment friendliness required for vehicles. To counteract these disadvantages of the existing intravehicle wired sensor network, Elbatt et al. proposed wireless sensor network as a potential way to replace the cable bundles for the transmission of data and control information between sensors and ECU [4]. A great challenge in constructing such an intravehicle wireless sensor network is to provide the same level of reliability, end-to-end latency, and data rate as what is offered by the current wiring system. Accordingly, to select a proper physical layer radio technology is crucial in the intravehicle propagation environment featuring short range and dense multipath. UWB technology is considered by us to be a competitive candidate for physical layer solution in constructing such an intravehicle wireless sensor network due to its robustness in solving multipath fading problem, low power consumption, resistance to narrow band interference, safe and high rate of data transmission as well as free availability of bandwidth.

UWB signal is defined as the wireless radio which takes a bandwidth larger than 500 MHz or a fractional bandwidth greater than 25%. In USA, FCC authorized the use of UWB signals in the frequency range between 3.1 GHz and 10.6 GHz with a power spectral density emission limited within −41.3 dBm/MHz [5]. Because UWB technology takes extremely wide transmission bandwidth, it provides fine

delay resolution in time domain, which in turn results in the lack of significant multipath fading. At the same time, UWB signals also demonstrate strong resistance to narrowband interference. These features make UWB a promising technique for implementing the intravehicle wireless sensor network. In order to design a UWB communication system, it is important to understand the UWB signal propagation characteristics in the desired environment. To date, lots of measurement experiments have already been performed in outdoor and indoor environments [6–10]. Moreover, channel models are available to describe the UWB propagation in these environments. In order to form physical layer standards for WPAN high-rate and low-rate applications, IEEE 802.15.3a and IEEE 802.15.4a channel modeling subgroups developed their UWB channel models, respectively [11, 12]. However, very little measuring or modeling work has been reported for intravehicle environment. The only reported effort relevant to the UWB propagation in vehicle environment is from [13]. But in that paper, the measurement is taken for an armored military vehicle, which is different from commercial vehicles in both size and equipments. Furthermore, the commercial vehicle sensors are normally located at such positions like wheel axis or engine compartment and so forth, but the measuring positions in [13] are either inside the passenger compartment or outdoors in proximity to the vehicle, which are very different from where commercial vehicle sensors are deployed.

In this paper, we report our UWB measurement conducted in commercial vehicle environment. The goal is to understand the intravehicle UWB propagation characteristics and develop a suitable channel model based on statistical analysis of the measured data. The paper is organized in the following way. Section 2 describes the measurement experiments. The deconvolution technique used to derive channel impulse responses is given in Section 3. Description of the channel models can be found in Section 4. The statistical calculation of multipath channel model parameters is described in Section 5. Path loss is calculated in Section 6. Finally, Section 7 summarizes the channel measurement and modeling results.

2. Intravehicle UWB Propagation Measurement

The measurement is performed in time domain by sounding the channel with narrow pulses and recording its response with a digital oscilloscope. Figure 1 is the block diagram illustrating the connections of the measurement apparatus shown in Figure 2. At the transmitting side, a Wavetek sweeper and an impulse generator from picosecond work together to create narrow pulses of width 100 picoseconds. These pulses are fed into a scissors-type antenna. At the receiving side, a digital oscilloscope of 15 GHz bandwidth from Tektronix (Org, USA) is connected to the receiving antenna to record the received signals. For the purpose of synchronization, three cables of same length are employed. The first cable connects the impulse generator output to the transmitting antenna, the second one lies between the receiving antenna and the signal input of the oscilloscope, and the third one is used to connect the impulse generator output to the trigger input of the oscilloscope. In this way, it is ensured that all recorded waveforms at the oscilloscope have the same reference point in time; hence, relative delays of signals arriving at the receiver via different propagation paths can be measured.

The experiment was conducted on the second floor of a large empty three-story parking building constructed from cement and mental. Measurement data were collected for a Ford Taurus and a GM Escalade when they were parked in the middle of the building, more than 6 meters away from any building wall. Figure 3 shows the building structure and the Escalade in the experiment. For each vehicle, the measurement was performed in two environments.

In the first environment, both the transmitting and the receiving antennas are beneath the chassis and 15 cm above the ground. They are set to face each other, and the line-of-sight (LOS) path always exists. Figure 4 illustrates the arrangement of the antennas' locations. For each vehicle, the transmitting antenna is fixed at location TX in the front, just beneath the engine compartment. The receiving antenna has been moved to ten different spots, namely, RX0-RX9. Five of them are located in a row along the left side of the car, with equidistance of 70 cm for the Taurus and 80 cm for the Escalade between the neighboring spots. The other five sit symmetrically along the right side of the car. Distance between TX and RX1 is 45 cm for the Taurus and 50 cm for the Escalade. In addition, RX0, RX1, RX8, and RX9 are located very close to the axes of the corresponding wheels. For each position, ten received waveforms are recorded by the oscilloscope when pulses are transmitted repeatedly. When the measurement is being taken, except the carton or package tape for supporting or attaching the antennas to the chassis, there is no other object lying in the space between the metal chassis and the cement ground. UWB propagation in this environment is measured because there are such sensors as wheel speed detectors installed at the wheel axes in modern vehicles. Sensor signals are transmitted via cables to the ECU, normally located in the front of a car. UWB transmission beneath the chassis is considered by us to be an attractive way of transmitting such sensor signals from the wheel axes or other parts of a vehicle to the ECU.

In the second environment, for each car, the two antennas are put inside the engine compartment with the hood closed. The positions of antennas highly depend on the available space in the compartment. Due to the difference between engine compartment structures of Taurus and Escalade, the arrangement of antenna positions is different as shown in Figure 5. But for both cars, the transmitting antenna is fixed, and the receiving antenna have been moved to different spots. Ten waveforms are recorded for each position of the receiving antenna. The engine compartments are full of metal auto components, and there are always iron parts sitting between the antennas. Measurement data are collected for this environment because some sensors like temperature detectors are located in the engine compartment.

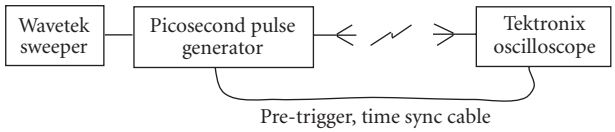

Figure 1: Connections of channel sounding apparatus.

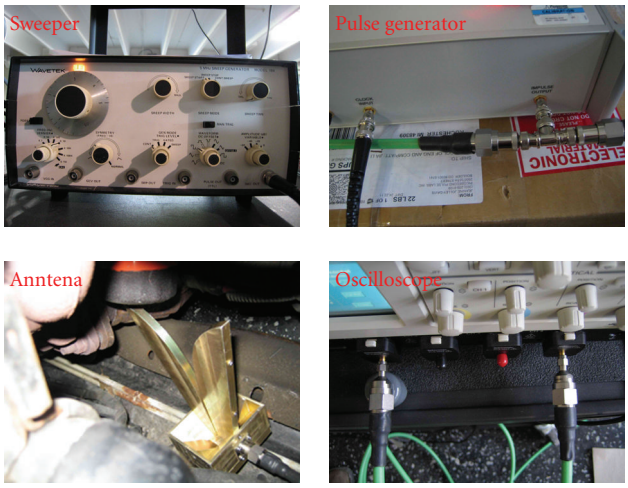

Figure 2: Channel sounding apparatus.

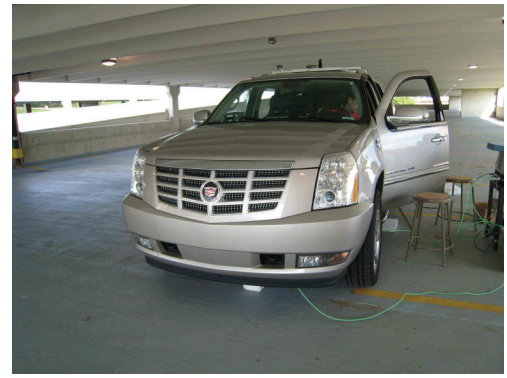

Figure 3: Parking building and a test vehicle.

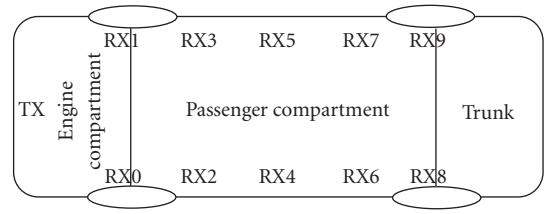

Figure 4: Antenna locations for the measurements beneath the chassis.

3. Channel Deconvolution

A channel can be characterized by its impulse responses (IR) in time domain. Each measured waveform is the convolution of the UWB channel IR, the sounding pulse, and the IR of the apparatus including the antennas, the cables, and the oscilloscope. We can apply deconvolution to get the channel impulse response from the measured data. In this paper, the subtractive deconvolution technique, also called CLEAN algorithm, is employed. CLEAN algorithm was originally used in radio astronomy to reconstruct images [14, 15]. Later it was used to find the channel impulse response. As is described by Vaughan and Scott in their paper [16], when CLEAN algorithm is used as a way of deconvolution, it assumes that any measured multipath signal $r(t)$ is the sum of a pulse shape $p(t)$. The channel impulse response is deconvolved by iteratively subtracting $p(t)$ from $r(t)$ until the remaining energy of $r(t)$ falls below a threshold. In our case, $p(t)$ is the waveform recorded by the oscilloscope when the two antennas are set to be one meter above the ground and one meter away from each other. The shape of $p(t)$ is shown in Figure 6. In detail, the algorithm is summarized as follows [16]:

(1) initialize the dirty signal with $d(t) = r(t)$ and the clean signal with $c(t) = 0$;

(2) initialize the damping factor γ which is usually called loop gain and the detection threshold T which is used to control the stopping time of the algorithm;

(3) calculate $x(t) = p(t) \overline{\otimes} d(t)$, where $\overline{\otimes}$ represents the normalized cross correlation;

(4) find the peak value P and its time position τ in $x(t)$;

(5) if the peak signal P is below the threshold T, stop the iteration;

(6) clean the dirty signal by subtracting the multiplication of $p(t)$, P, and γ : $d(t) = d(t) - p(t-\tau) \cdot P \cdot \gamma$;

(7) update the clean signal by $c(t) = c(t) + P \cdot \gamma \cdot \delta(t-\tau)$;

(8) loop back to step (3);

(9) $c(t)$ is the channel impulse response.

The impulse response generated by this algorithm is determined by the value of the loop gain γ and the threshold of the stop criteria T. In our deconvolution process, based on the balance of the computation time and the algorithm performance, γ is set to 0.01 and T is set to 0.04. Figure 7 shows an example of a received signal from beneath the chassis and the impulse response obtained via CLEAN algorithm. Each vertical line in the impulse response figure represents a multipath component (MPC) whose relative time delay and strength are indicated by the time position and amplitude of the line. An example of measured waveforms from the UWB propagation inside the engine compartments is shown in Figure 8 together with the impulse response. Observation of the recorded waveforms and the deconvolved impulse responses reveals that paths arrive in clusters in this environment. But for the measurements taken beneath the chassis, there is no clustering phenomenon observed. This observation is consistent with the structure of the channels. Normally, the multiple rays reflected from a nearby obstacle arrive with close delays, tending to form a cluster. Strong reflections from another obstacle separated in distance tend

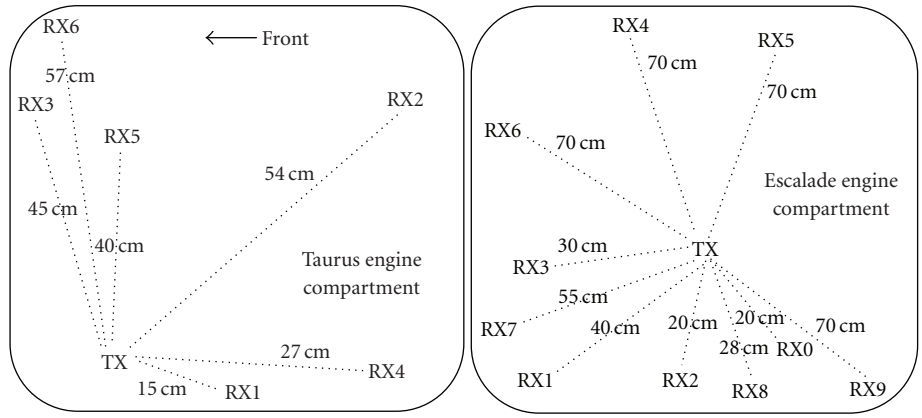

Figure 5: Antenna locations for the measurements inside the engine compartments.

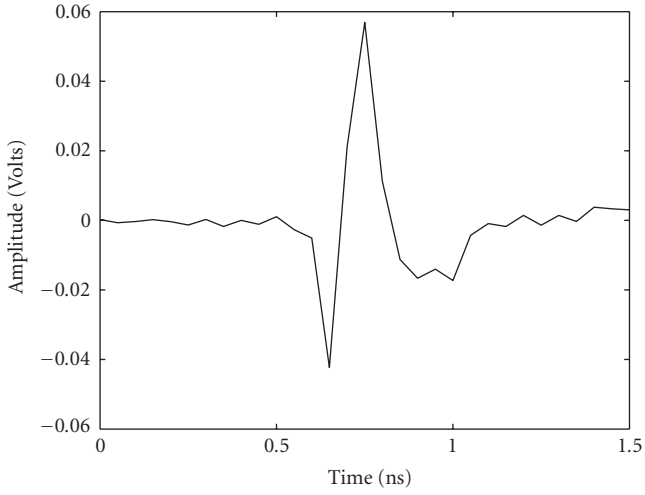

Figure 6: Received UWB signal when receiving antenna is 1 m away from transmitting antenna.

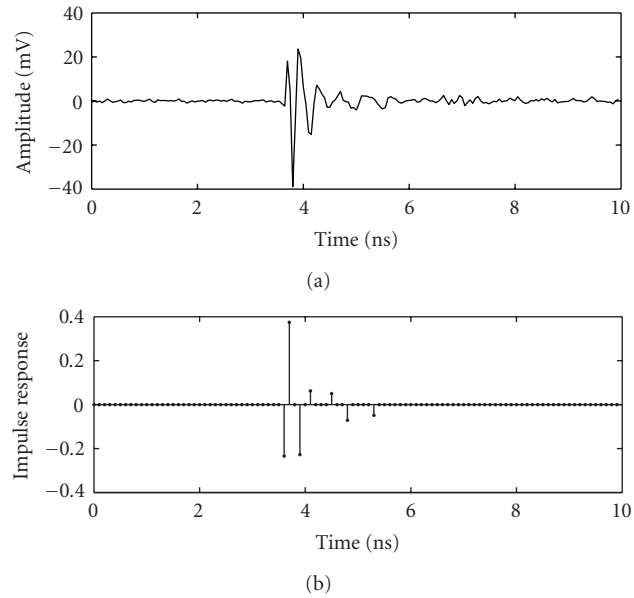

Figure 7: Example of received waveform and the corresponding CIR for under chassis environment.

to form another cluster. The combined effects result in multiple clusters in an impulse response. Inside the engine compartments, there are auto parts sitting between or nearby the transmitter and the receiver. But the channel beneath the chassis only consists of the ground and the chassis, without other obstacles sitting in the vicinity of the transmitter or receiver. The lack of multiple scattering obstacles leads to the lack of multiple clusters in this environment.

4. Statistical Multipath Channel Models

Based on the observation that the clustering phenomenon exists for the UWB propagation inside the engine compartment but not for that under the chassis, different models should be used to describe the channels in these two environments. It is also observed in the experiments that for the same antenna position there are very tiny differences between the waveforms recorded at different time points when sequences of narrow pulses are transmitted periodically; thus the channels can be considered as time-invariant. We discuss the two channel models below.

4.1. UWB Propagation Beneath the Chassis. Narrowband propagation channel impulse response can be represented as

$$h(t) = \sum_{k=0}^{K} \alpha_k \exp(j\theta_k)\delta(t - \tau_k), \tag{1}$$

where K is the number of multipath components, α_k are the positive random path gains, θ_k are the phase shifts, and τ_k are the path arrival time delays of the multipath components [17, 18]. θ_k is considered to be a uniformly distributed random variable in the range of $[0, 2\pi)$. However, as stated in [19], for UWB channels, because of the frequency selectivity in the reflection, diffraction, or scattering processes, MPCs

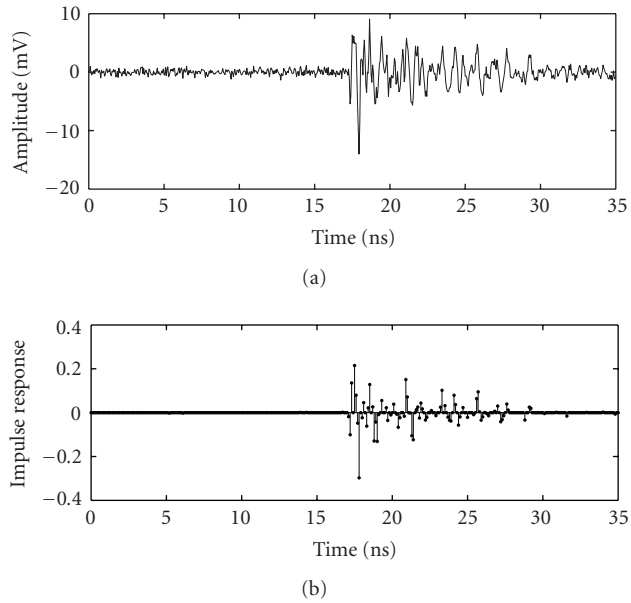

Figure 8: Example of received waveform and the corresponding CIR for engine compartment environment.

experience distortions and the impulse response should be written as

$$h(t) = \sum_{k=0}^{K} \alpha_k \chi_k \exp(j\theta_k)\delta(t - \tau_k), \tag{2}$$

in which χ_k denotes the distortion of the kth MPC. In this paper, for simplicity, the impulse response of the UWB propagation channel beneath the chassis is still described by (1), and the phase θ_k equiprobably takes the value 0 or π. In addition, the arrival of the paths is described as a Poisson process, and the distribution of arrival intervals is expressed as follows:

$$p(\tau_k \mid \tau_{k-1}) = \lambda \exp[-\lambda(\tau_k - \tau_{k-1})], \quad k > 0, \tag{3}$$

where λ is the path arrival rate [20].

As for the shape of the power delay profile (PDP), our measurement results from the chassis environment show that PDPs do not decay monotonically. Instead, each PDP has a rising edge at the beginning; it reaches the maximum later and decays after that peak. So we adopt the following function proposed in [21] to describe the mean power of the paths:

$$E\{\alpha_k^2\} = \Omega \cdot \left(1 - \chi \cdot \exp\left(-\frac{\tau_k}{\gamma_{\text{rise}}}\right)\right) \cdot \exp\left(-\frac{\tau_k}{\gamma}\right), \tag{4}$$

where τ_k is the arrival delay of the kth path relative to the first path, χ describes the attenuation of the first path, γ_{rise} determines how fast the PDP increases to the maximum peak, γ controls the decay after the peak, and Ω is the integrated energy of the PDP.

4.2. UWB Propagation Inside the Engine Compartment. The classical S-V channel model to account for the clustering of MPCs is expressed as

$$h(t) = \sum_{l=0}^{L} \sum_{k=0}^{K} \alpha_{kl} \exp(j\theta_{kl})\delta(t - T_l - \tau_{kl}), \tag{5}$$

where L is the number of clusters, K is the number of MPCs within a cluster, α_{kl} is the multipath gain of the kth path in the lth cluster, T_l is the delay of the lth cluster, that is, the arrival time of the first path within the lth cluster, assuming that the first path in the first cluster arrives at time zero, τ_{kl} is the delay of the kth path within the lth cluster, relative to the arrival time of the cluster, and θ_{kl} is the phase shift of the kth path within the lth cluster [20].

Similar to the chassis model, for simplicity, the MPC distortion of UWB signal mentioned in [19] is not considered in this paper, and (5) has been used to describe the UWB multipath propagation inside the engine compartment. The phases θ_{kl} are also considered to equiprobably equal 0 or π. In addition, the arrival of the clusters and the arrival of the paths within a cluster are described as two Poisson processes. Accordingly, the cluster interarrival time and the path interarrival time within a cluster obey exponential distribution described by the following two probability density functions [20]:

$$\begin{aligned} p(T_l \mid T_{l-1}) &= \Lambda \exp[-\Lambda(T_l - T_{l-1})], \quad l > 0, \\ p(\tau_{kl} \mid \tau_{(k-1)l}) &= \lambda \exp[-\lambda(\tau_{kl} - \tau_{(k-1)l})], \quad k > 0, \end{aligned} \tag{6}$$

where Λ is the cluster arrival rate, and λ is the path arrival rate within clusters.

Furthermore, S-V model assumes that the average power of both the clusters and the paths within the clusters decay exponentially as follows:

$$\overline{\alpha_{kl}^2} = \overline{\alpha_{00}^2} \exp\left(-\frac{T_l}{\Gamma}\right) \exp\left(-\frac{\tau_{kl}}{\gamma}\right), \tag{7}$$

where $\overline{\alpha_{00}^2}$ is the expected power of the first path in the first cluster, and Γ and γ are the power decay constants for the clusters and the paths within clusters, respectively. Normally γ is smaller than Γ, which means that the average power of the paths in a cluster decay faster than the first path of the next cluster.

5. Data Processing and Analysis

In this section, channel impulse responses are statistically analyzed to extract parameters for the channel models. In the processing of those PDPs showing clustering phenomenon, clusters are identified manually via visual inspection. Both the path arrival time and the variations in the amplitudes are considered in the cluster identification process. Generally speaking, when there is no overlap between neighboring clusters, MPCs having similar delays are grouped into a cluster. But when the overlap happens, path amplitude

variations will be considered in the identification of clusters. In such case, new clusters are identified at the points where there are big variations, normally sudden increase, in the path amplitudes.

5.1. RMS Delay Spread Distribution. Root-mean-square (RMS) delay spread is the standard deviation value of the delay of paths, weighted proportional to the path power. It is defined as

$$\tau_{\text{rms}} = \sqrt{\frac{\sum_k (t_k - t_1 - \tau_m)^2 \alpha_k^2}{\sum_k \alpha_k^2}}, \tag{8}$$

where t_k and t_1 are the arrival time of the kth path and the first path, respectively, α_k is the amplitude of the kth path, and τ_m is the mean excess delay defined as

$$\tau_m = \frac{\sum_k (t_k - t_1)\alpha_k^2}{\sum_k \alpha_k^2}. \tag{9}$$

RMS delay spread is considered to be a good measure of multipath spread. It indicates the potential of the maximum data rate that can be achieved without intersymbol interference (ISI) [18]. Generally, serious ISI is likely to occur when the symbol duration is less than ten times RMS delay spread. As an important characteristic of the multipath channel, RMS delay spread is calculated for each of our deconvolved channel impulse responses. The measured complementary cumulative distribution functions (CCDFs) of the RMS delay spread for the measurements taken beneath the Taurus and Escalade chassis are plotted in Figure 9, with their counterparts for the engine compartment measurements shown in Figure 10. The results show that the mean RMS delay spread in the Taurus and Escalade chassis environment is 0.3101 nanosecond and 0.4431 nanosecond, respectively. In the mean time, the engine compartment environment gives the empirical mean RMS delay spread of 1.5918 nanoseconds for Taurus and 1.7165 nanoseconds for Escalade. All of them are much less than those reported for indoor or outdoor environments, indicating less possibility of serious ISI [11]. Because the multipath delay spread decreases when the distance between the transmitter and receiver decreases [22], the small RMS delay spreads in our measurement result from the small distance between the antennas. In most cases, they are separated by less than 5 meters, which is much less than those of indoor or outdoor measurement environments. Furthermore, the lack of multiple reflecting obstacles for the chassis environment makes the RMS delay spread even smaller.

5.2. Interpath and Intercluster Arrival Times. As stated in Section 4, the cluster arrival and intracluster path arrival in S-V model are considered to be Poisson arrival processes with fixed rate Λ and λ, respectively. Accordingly, their interarrival intervals have exponential distributions. The

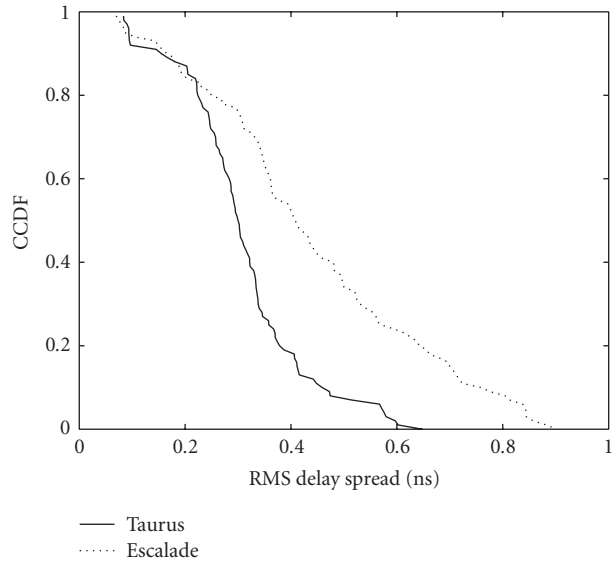

Figure 9: CCDF of the RMS delay spread for UWB propagation beneath the chassis.

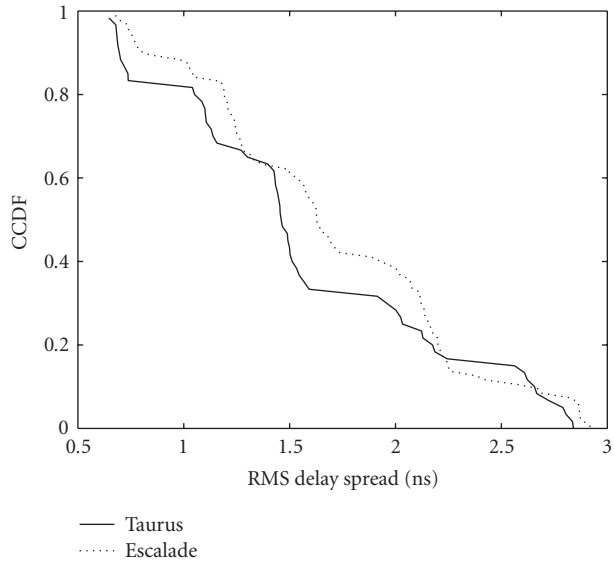

Figure 10: CCDF of the RMS delay spread for UWB propagation inside the engine compartments.

method to estimate λ and Λ is to get the empirical cumulative distribution functions (CDFs) of the path and cluster arrival intervals from the measurement data and then find the exponential distribution functions best fitting them. λ or Λ is just the reciprocal of the mean value of such an exponential distribution function. Following this procedure, $1/\lambda$ for the measurements beneath the Taurus chassis is determined to be 0.2846 nanosecond, and it is 0.4101 nanosecond for those beneath the Escalade chassis. In addition, for the data measured inside the Taurus engine compartment, $1/\lambda$ is 0.2452 nanosecond, and $1/\Lambda$ equals 3.0791 nanoseconds. Their corresponding values for the Escalade are 0.3185 nanosecond and 3.2575 nanoseconds, respectively. The semilog plots for

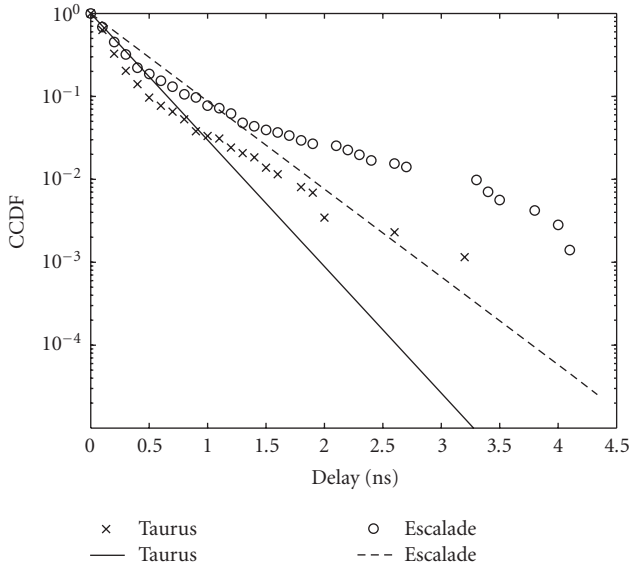

Figure 11: CCDF of interpath arrival intervals and the best-fit exponential distributions for measurements beneath the chassis.

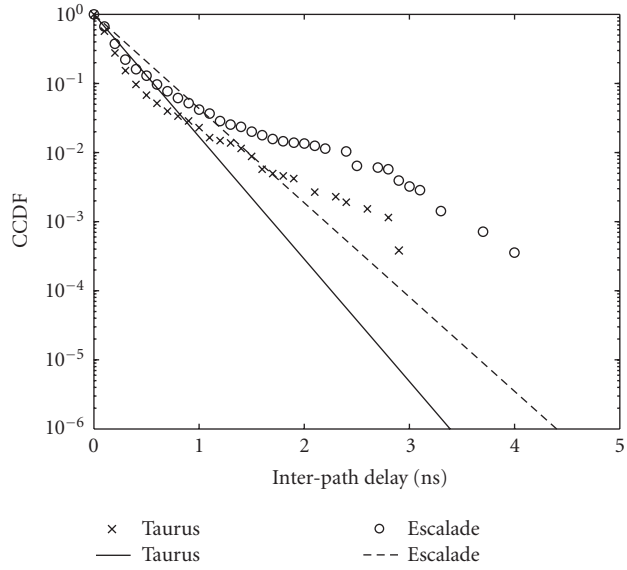

Figure 12: CCDF of interpath arrival intervals and the best-fit exponential distributions for measurements inside the engine compartments.

the CCDFs of these interarrival intervals with their best-fit exponential distributions are shown in Figures 11, 12, and 13. In these figures, each best-fit exponential distribution is found in the meaning of maximum likelihood estimation, and their mean values just equal the reciprocal of the path or cluster arrival rates. It can be observed that both the path arrival rates and the cluster arrival rates are larger than those reported for indoor or outdoor environments [9, 10, 12]. The reason for these faster arrival rates is due to the much shorter range of the UWB propagation in the intravehicle environment. In addition, the fine resolution with a bin width of 0.1 nanosecond used by us contributes to the number of resolved paths, which in turn also contributes to the faster path arrival rates.

5.3. Distributions of Path and Cluster Amplitudes. In narrowband models, the amplitudes of the multipath components are usually assumed to follow Rayleigh distribution, but this is not necessarily the best description of UWB MPCs amplitudes. Due to the ultra-wide bandwidth of the UWB signals, the time delay difference between resolvable paths, which normally equals the reciprocal of the bandwidth, is much smaller than that of the narrowband signals. As a result, each observed UWB MPC is the sum of a much smaller number of unresolvable paths. It is highly possible that the amplitude distribution is not Rayleigh. To evaluate the distributions of UWB path and cluster amplitudes, in this paper we match the empirical CDF of the measured amplitudes against Rayleigh and lognormal to find out which one is a better fit.

Before the empirical CDF of the path or cluster amplitudes is calculated, each CIR is normalized by setting the amplitude of the peak path to be one, then the amplitudes of the other paths in this CIR are expressed in values relative to it. In addition, the peak amplitude within a

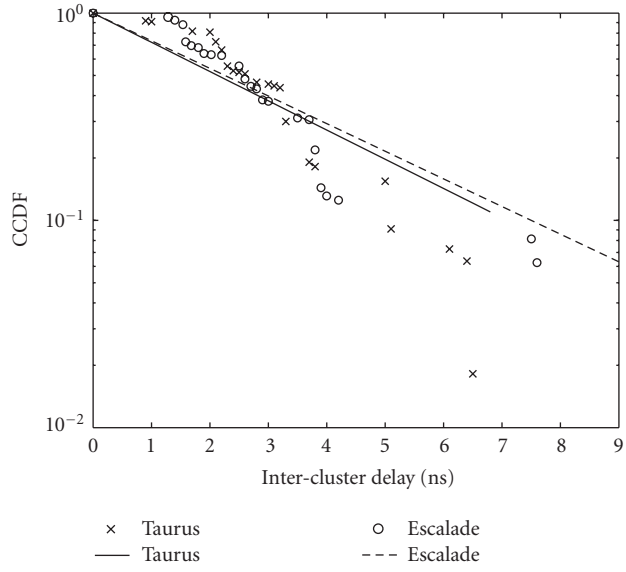

Figure 13: CCDF of intercluster arrival intervals and the best-fit exponential distributions for measurements inside the engine compartments.

cluster is identified as the amplitude of the cluster. The Rayleigh distribution and lognormal distribution best fitting the empirical CDFs of these amplitudes in the meaning of maximum likelihood estimation are found. The probability density function for Rayleigh distribution is

$$f(x;\sigma) = \frac{x \exp\left(-x^2/2\sigma^2\right)}{\sigma^2}, \quad x \in [0,\infty), \tag{10}$$

Table 1: Standard deviations of best-fit Rayleigh and lognormal distributions to the CDFs of path and cluster amplitudes.

CDF	Standard deviation σ	
	Rayleigh	Lognormal
Path amplitude (Taurus chassis)	0.3481	7.5688
Path amplitude (Taurus engine compartment)	0.2122	11.0571
Cluster amplitude (Taurus engine compartment)	0.5153	5.1993
Path amplitude (Escalade chassis)	0.3348	6.5672
Path amplitude (Escalade engine compartment)	0.2149	11.3850
Cluster amplitude (Escalade engine compartment)	0.5401	5.2763

where σ is the standard deviation. For lognormal distribution, the probability density function is given by

$$f(x;\mu,\sigma) = \frac{\exp\left[-\left(\ln(x)-\mu\right)^2/2\sigma^2\right]}{x\sigma\sqrt{2\pi}}, \quad x \in [0,\infty), \tag{11}$$

where μ is the expected value, and σ is the standard deviation, respectively. For our measurements from beneath the chassis and inside the engine compartments, standard deviations of the best-fit Rayleigh and lognormal distributions are found and listed in Table 1. In the mean time, CDFs of the amplitudes for these measurements are plotted in Figures 14, 15, 16, 17, 18, and 19, with their best-fit Rayleigh and lognormal distributions overlaid. In each figure, it can be easily observed that the best-fit lognormal distribution curve is closer to the distribution curve of the measured data than that of the best-fit Rayleigh distribution. Calculation of the root mean square errors (RMSEs) for the best-fit Rayleigh and the best-fit lognormal distribution shows that the latter is a better fit in all cases.

5.4. Path and Cluster Power Decay. On the one hand, to calculate the PDP model parameters χ, γ, and γ_{rise} defined in (4) for the measured data from beneath the chassis, the deconvolved CIRs are normalized in a way so that for each of them the integrated energy equals one and the first path arrives at time zero. The average normalized path powers versus their relative delays are plotted in Figure 20 for the Taurus and in Figure 23 for the Escalade. Values of χ, γ_{rise}, and γ are found by computing the curve best fitting these power values in the least squares sense. As illustrated in Figures 20 and 23, such curves give χ, γ, and γ_{rise} the values of 0.9452, 0.2117, and 0.2524 nanosecond for the Taurus and 0.9240, 0.2141, and 0.2997 nanosecond for the Escalade, respectively.

On the other hand, to get the path power decay constant γ for the measured data from the engine compartments, normalization is performed on all clusters in the CIRs, so that the first path in each cluster has an amplitude of one and a time delay of zero. Then powers of the paths within these normalized clusters are calculated and superimposed in Figures 21 and 24 for the Taurus and the Escalade. The power decay constant γ is found by computing a linear curve best fitting these powers in the least squares sense, and γ just equals the absolute reciprocal of the curve's slope. In Figures 21 and 24, this curve is shown as the solid line, and it gives the intracluster path power decay constant γ a value of 1.0840 nanoseconds for the Taurus and 1.9568

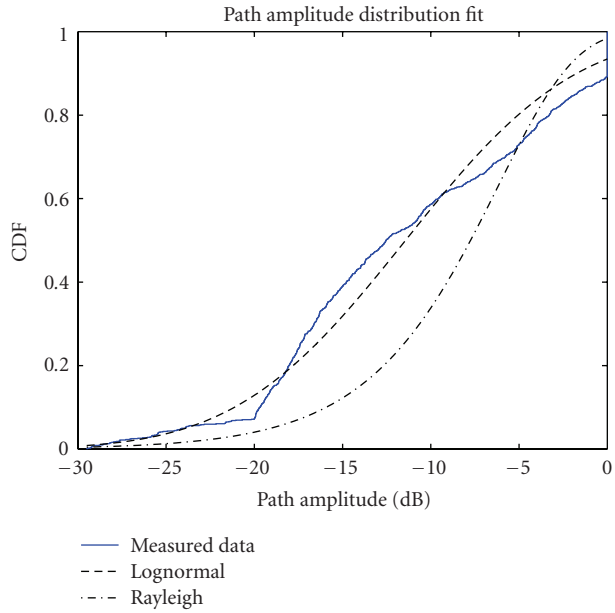

Figure 14: Path amplitudes CDF with the best-fit Rayleigh (RMSE = 1.1789) and lognormal (RMSE = 0.0489) distributions for measurements beneath the Taurus chassis.

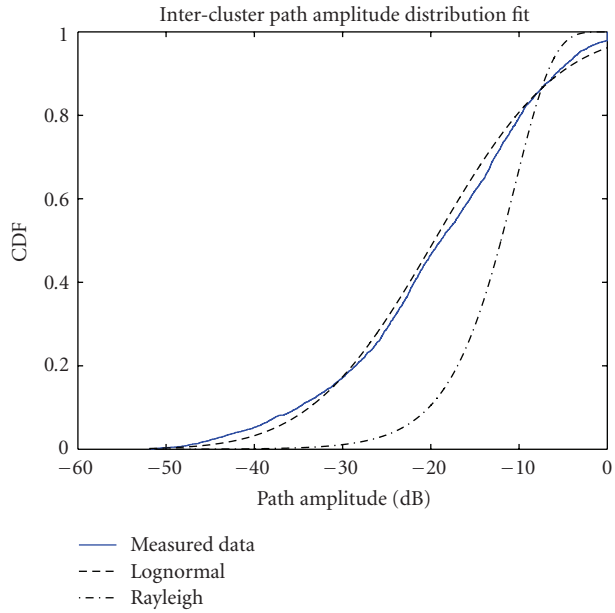

Figure 15: Intra-cluster path amplitudes CDF with the best-fit Rayleigh (RMSE = 0.2357) and lognormal (RMSE = 0.0239) distributions for measurements inside the Taurus engine compartment.

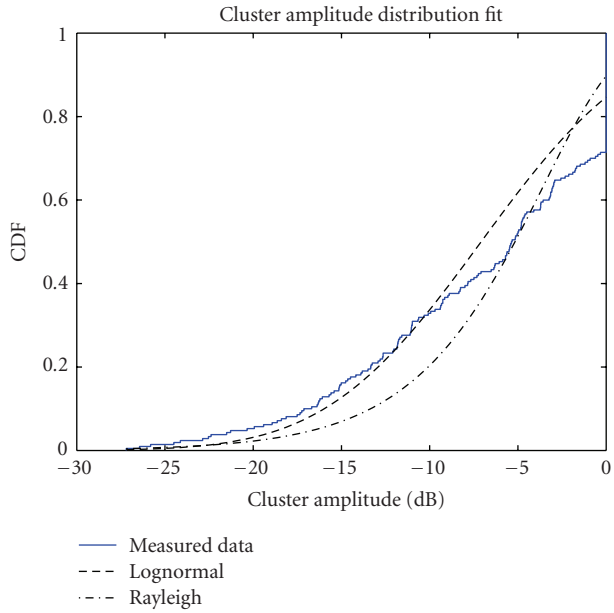

Figure 16: Cluster amplitudes CDF with the best-fit Rayleigh (RMSE = 0.0840) and lognormal (RMSE = 0.0661) distributions for measurements inside the Taurus engine compartment.

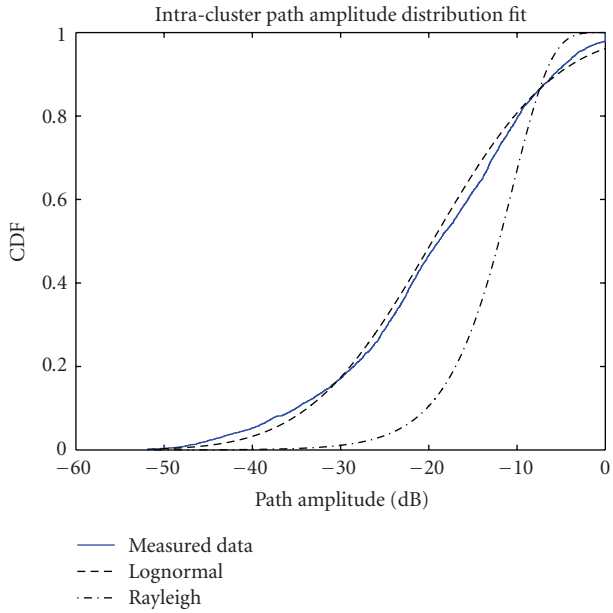

Figure 18: Intracluster path amplitudes CDF with the best-fit Rayleigh (RMSE = 0.2284) and lognormal (RMSE = 0.0319) distributions for measurements inside the Escalade engine compartment.

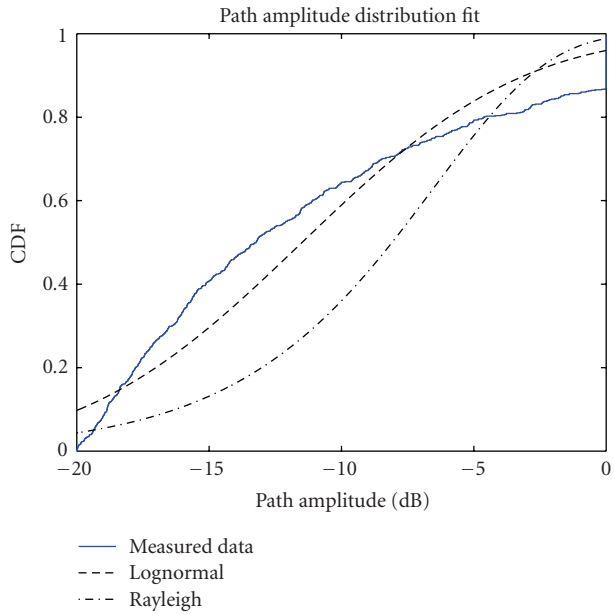

Figure 17: Path amplitudes CDF with the best-fit Rayleigh (RMSE = 0.2078) and lognormal (RMSE = 0.0726) distributions for measurements beneath the Escalade chassis.

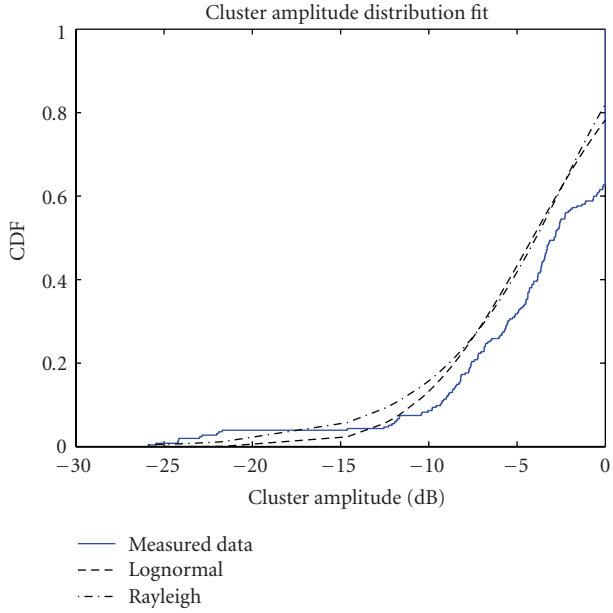

Figure 19: Cluster amplitudes CDF with the best-fit Rayleigh (RMSE = 0.0891) and lognormal (RMSE = 0.0884) distributions for measurements inside the Escalade engine compartment.

nanoseconds for the Escalade. Similarly, in order to get the cluster power decay constant Γ, each CIR is normalized in a way so that its first cluster has an amplitude of one and an arrival time of zero. Here, cluster amplitude is defined as the peak amplitude within a cluster, and cluster delay is defined as the arrival time of the first path within the cluster, respectively. Figure 22 shows the superimposition of the cluster powers for the measurements of the Taurus engine compartment, and Figure 25 shows that of the Escalade engine compartment. The best-fit curves to these cluster powers which are shown as the solid lines in the figures determine the cluster decay constant Γ to be 3.0978 nanoseconds for the Taurus and 3.1128 nanoseconds for the Escalade, respectively. It is observed that both γ and Γ are smaller than their corresponding values reported in [12] for indoor or outdoor environments, which means faster power

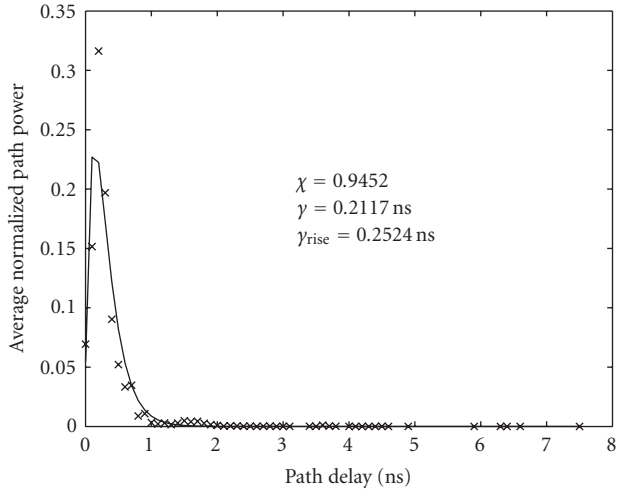

Figure 20: Average normalized path power decay for measurements beneath the Taurus chassis.

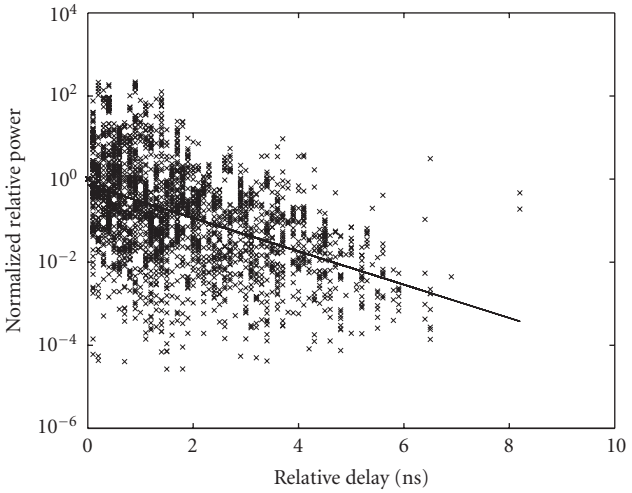

Figure 21: Normalized path power decay for measurements from the Taurus engine compartment.

decay in the engine compartment. Again, this is caused by the much smaller space in the engine compartment.

6. Path Loss

Path loss describes the ratio of the transmitted signal power to the received signal power. The relation between path loss and the distance is normally described as follows [12, 23]:

$$\mathrm{PL}(d) = \mathrm{PL}_0 - 10 \cdot n \cdot \log_{10}\left(\frac{d}{d_0}\right) + S, \qquad (12)$$

in which PL_0 is the path loss at the reference distance d_0 of 1 m, n is the path loss exponent, d is the distance between the transmitting and the receiving antenna at each measurement spot, and S is a zero mean random variable which has Gaussian distribution with standard deviation σ_s. To evaluate the path loss exponent, the average received

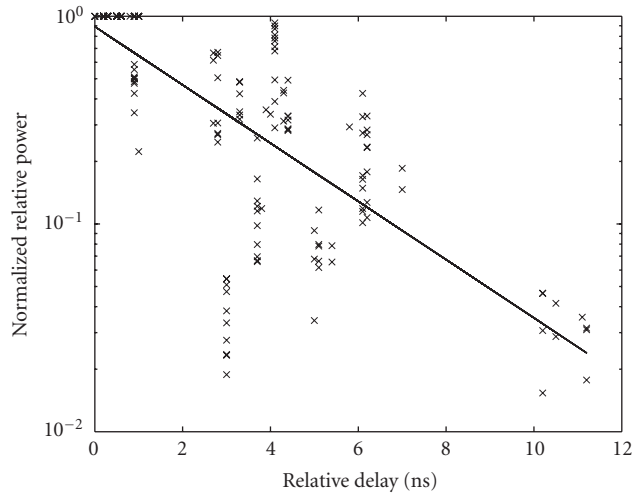

Figure 22: Normalized cluster power decay for measurements from the Taurus engine compartment.

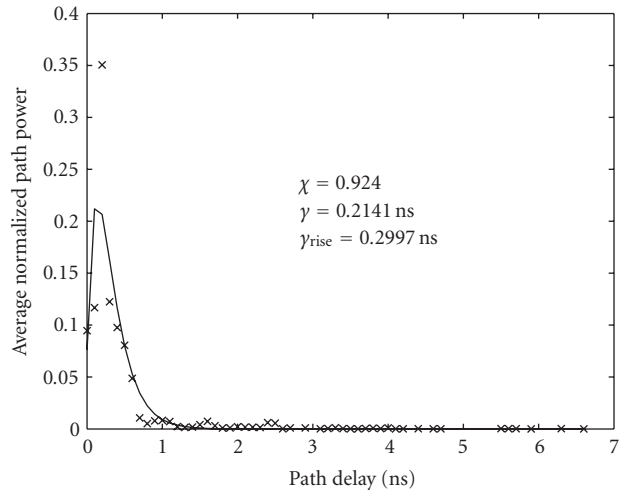

Figure 23: Average normalized path power decay for measurements beneath the Escalade chassis.

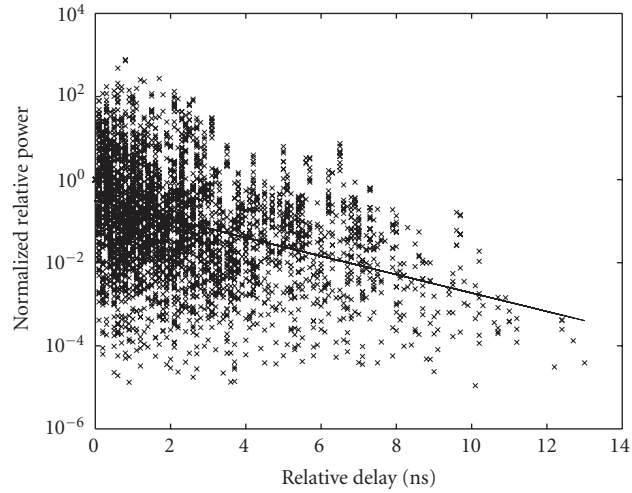

Figure 24: Normalized path power decay for measurements from the Escalade engine compartment.

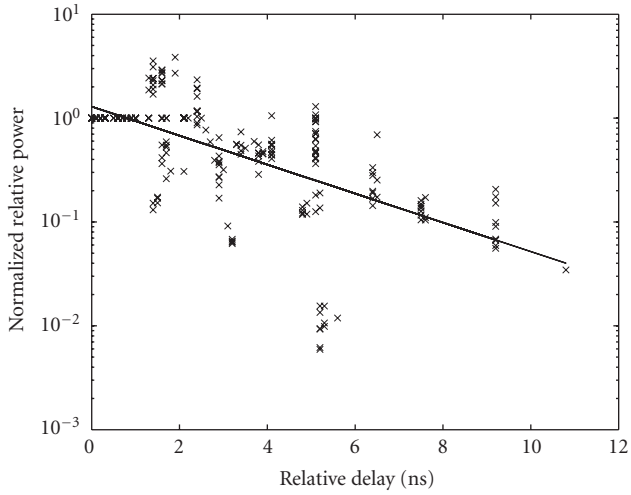

Figure 25: Normalized cluster power decay for measurements from the Escalade engine compartment.

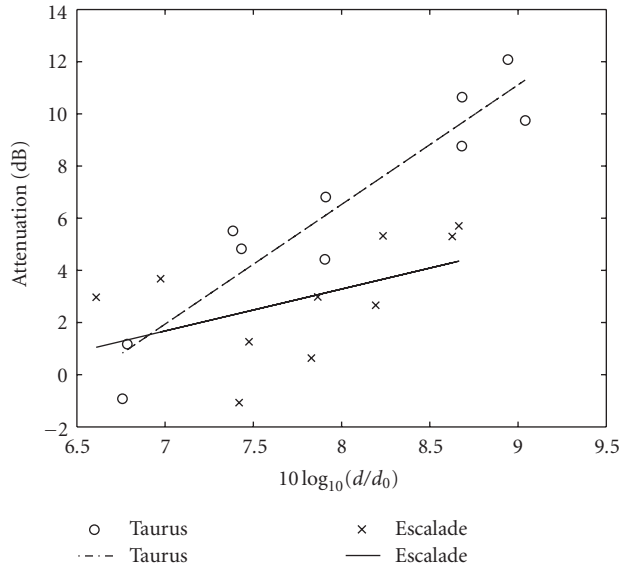

Figure 26: Path loss beneath the chassis.

Table 2: Path loss

Path loss	Beneath chassis		Engine compartment	
	Taurus	Escalade	Taurus	Escalade
PL_0 (dB)	30.15	9.57	4.86	6.32
n	4.58	1.61	1.21	1.51
σ_s	1.34	1.92	4.20	3.00

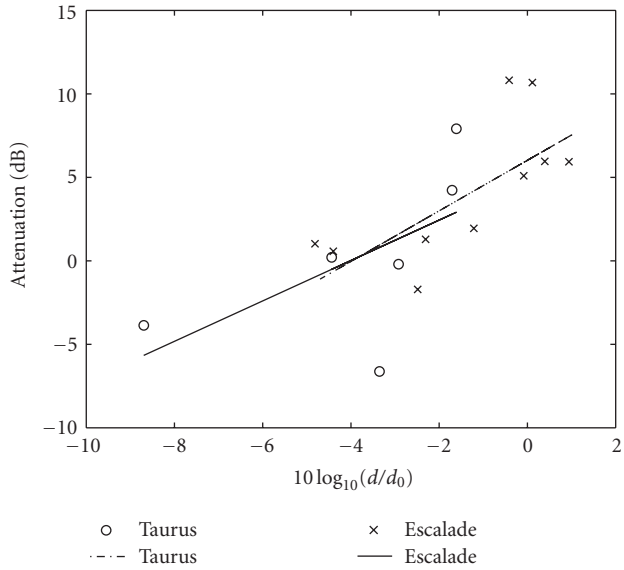

Figure 27: Path loss inside the engine compartments.

energy at each measurement position is calculated directly from the impulse responses. Then the path loss versus $\log_{10}(d/d_0)$ is plotted in Figures 26 and 27. A least square fit computation is performed in order to get the value of n for the chassis and engine compartment environments. The extracted path loss parameters from the measurement data are listed in Table 2. Values of these parameters are comparable with those reported for indoor or outdoor UWB measurements [12]. However, it is observed that path loss beneath the Taurus chassis shows big difference from that beneath the Escalade chassis. This is caused by the large path loss values for position RX0 and position RX1 beneath the Escalade chassis. For these two positions, half the receiving antenna was above the Escalade front wheel axis and half was not, when the measurements were being performed. As a result, part of the energy was blocked by the axis and the chassis sitting between the transmitting antenna which was below the chassis plane, and the receiving antenna half of which was above the chassis plane. If measurement data from these two positions are excluded when calculating the path loss for the Escalade chassis environment, the extracted PL_0 equals 35.15 dB, n equals 4.73, and σ_s equals 1.06.

Equation (12) describes the path loss dependence on distance. For UWB, there is also frequency dependency in the propagation, and the path loss is also a function of frequency [19]. The frequency dependency of the UWB path loss is not included in this paper and will be studied in the future.

7. Summary

The main goal of our work is to understand the UWB propagation in intravehicle environment. In this paper, we report our UWB measurement results and the effort to model the multipath propagation channels in two commercial vehicles. Measurements are taken either from beneath the chassis environment or from inside the engine compartment environment. We use different channel models to describe the UWB propagation in these two environments considering the difference in clustering phenomenon. In addition, statistical analysis is applied to the measurement data to derive the model parameters. It is exhibited that in the intravehicle environment, the path or cluster arrival rates are greatly larger than those reported for indoor or outdoor

environments while the path or cluster power decay constants are smaller. In addition, the RMS delay spreads from our measurements are also less than those reported for the indoor UWB propagation, indicating potential for smaller symbol duration when avoiding intersymbol interference, hence potential for higher data rate [11].

References

[1] T. Costlow, "Sensing significant growth," *SAE International*, pp. 74–78, May 2004.

[2] W. J. Fleming, "Overview of automotive sensors," *IEEE Sensors Journal*, vol. 1, no. 4, pp. 296–308, 2001.

[3] G. Leen and D. Heffernan, "Vehicles without wires," *Computing & Control Engineering Journal*, vol. 12, no. 5, pp. 205–211, 2001.

[4] T. Elbatt, C. Saraydar, M. Ames, and T. Talty, "Potential for intra-vehicle wireless automotive sensor networks," in *Proceedings of IEEE Sarnoff Symposium*, pp. 1–4, Princeton, NJ, USA, March 2006.

[5] First report and order 02-48, Federal Communications Commission, 2002.

[6] G. Schiavone, P. Wahid, R. Palaniappan, J. Tracy, E. van Doorn, and B. Lonske, "Outdoor propagation analysis of ultra wide band signals," in *Proceedings of IEEE Antennas and Propagation Society International Symposium (AP-S '03)*, vol. 2, pp. 999–1002, Columbus, Ohio, USA, June 2003.

[7] M. Z. Win, F. Ramirez-Mireles, R. A. Scholtz, and M. A. Barnes, "Ultra-wide bandwidth (UWB) signal propagation for outdoor wireless communications," in *Proceedings of the 47th IEEE Vehicular Technology Conference (VTC '97)*, vol. 1, pp. 251–255, Phoenix, Ariz, USA, May 1997.

[8] J. Choi, N.-G Kang, Y.-S Sung, and S.-C Kim, "Empirical ultra wide band channel model for short range outdoor environments," in *Proceedings of the 65th IEEE Vehicular Technology Conference (VTC '07)*, pp. 1579–1583, Dublin, Ireland, April 2007.

[9] R. J.-M. Cramer, R. A. Scholtz, and M. Z. Win, "Evaluation of an ultra-wide-band propagation channel," *IEEE Transactions on Antennas and Propagation*, vol. 50, no. 5, pp. 561–570, 2002.

[10] Q. Spencer, M. Rice, B. Jeffs, and M. Jensen, "A statistical model for angle of arrival in indoor multipath propagation," in *Proceedings of the 47th IEEE Vehicular Technology Conference (VTC '97)*, vol. 3, pp. 1415–1419, Phoenix, Ariz, USA, May 1997.

[11] J. Foerster, "Channel modeling sub-committee report final," IEEE P802.15-02/490r1-SG3a, February 2003.

[12] A. F. Molisch, K. Balakrishnan, D. Cassioli, et al., "IEEE 802.15.4a channel model—final report," IEEE 802.15-04-0662-00-004a, November 2004.

[13] P. C. Richardson, W. Xiang, and W. Stark, "Modeling of ultra-wideband channels within vehicles," *IEEE Journal on Selected Areas in Communications*, vol. 24, no. 4, pp. 906–912, 2006.

[14] J. A. Högbom, "Aperture synthesis with a non-regular distribution of interferometer baselines," *Astronomy and Astrophysics Supplement Series*, vol. 15, pp. 417–426, 1974.

[15] R. H. T. Bates and M. J. McDonnell, *Image Restoration and Reconstruction*, Oxford Engineering Science Series, Clarendon Press, Oxford, UK, 1986.

[16] R. G. Vaughan and N. L. Scott, "Super-resolution of pulsed multipath channels for delay spread characterization," *IEEE Transactions on Communications*, vol. 47, no. 3, pp. 343–347, 1999.

[17] J. G. Proakis, *Digital Communications*, McGraw-Hill, New York, NY, USA, 5th edition, 2007.

[18] H. Hashemi, "The indoor radio propagation channel," *Proceedings of the IEEE*, vol. 81, no. 7, pp. 943–968, 1993.

[19] A. F. Molisch, "Ultrawideband propagatiton channels-theory, measurement, and modeling," *IEEE Transactions on Vehicular Technology*, vol. 54, no. 5, pp. 1528–1545, 2005.

[20] A. Saleh and R. Valenzuela, "A statistical model for indoor multipath propagation," *IEEE Journal on Selected Areas in Communications*, vol. 5, no. 2, pp. 128–137, 1987.

[21] A. F. Molisch, D. Cassioli, C.-C. Chong, et al., "A comprehensive standardized model for ultrawideband propagation channels," *IEEE Transactions on Antennas and Propagation*, vol. 54, no. 11, pp. 3151–3166, 2006.

[22] M. Ghavami, L. B. Michael, and R. Kohno, *Ultra Wideband Signals and Systems in Communication Engineering*, John Wiley & Sons, New York, NY, USA, 2004.

[23] J. D. Parsons, *The Mobile Radio Propagation Channel*, John Wiley & Sons, New York, NY, USA, 2nd edition, 2000.

EURASIP Journal on Advances in Signal Processing

Special Issue on Advances in Signal Processing for Maritime Applications

Call for Papers

The maritime domain continues to be important for our society. Significant investments continue to be made to increase our knowledge about what "happens" underwater, whether at or near the sea surface, within the water column, or at the seabed. The latest geophysical, archaeological, and oceanographical surveys deliver more accurate global knowledge at increased resolutions. Surveillance applications allow dynamic systems, such as marine mammal populations, or underwater intruder scenarios, to be accurately characterized. Underwater exploration is fundamentally reliant on the effective processing of sensor signal data. The miniaturization and power efficiency of modern microprocessor technology have facilitated applications using sophisticated and complex algorithms, for example, synthetic aperture sonar, with some algorithms utilizing underwater and satellite communications. The distributed sensing and fusion of data have become technically feasible, and the teaming of multiple autonomous sensor platforms will, in the future, provide enhanced capabilities, for example, multipass classification techniques for objects on the sea bottom. For such multiplatform applications, signal processing will also be required to provide intelligent control procedures.

All maritime applications face the same difficult operating environment: fading channels, rapidly changing environmental conditions, high noise levels at sensors, sparse coverage of the measurement area, limited reliability of communication channels, and the need for robustness and low energy consumption, just to name a few. There are obvious technical similarities in the signal processing that have been applied to different measurement equipment, and this Special Issue aims to help foster cross-fertilization between these different application areas.

This Special Issue solicits submissions from researchers and engineers working on maritime applications and developing or applying advanced signal processing techniques. Topics of interest include, but are not limited to:

- Sonar applications for surveillance and reconnaissance
- Radar applications for measuring physical parameters of the sea surface and surface objects
- Nonacoustic data processing and sensor fusion for improved target tracking and situational awareness
- Underwater imaging for automatic classification
- Signal processing for distributed sensing and networking including underwater communication
- Signal processing to enable autonomy and intelligent control

Before submission authors should carefully read over the journal's Author Guidelines, which are located at http://www.hindawi.com/journals/asp/guidelines.html. Authors should follow the EURASIP Journal on Advances in Signal Processing manuscript format described at the journal site http://www.hindawi.com/journals/asp/. Prospective authors should submit an electronic copy of their complete manuscript through the journal Manuscript Tracking System at http://mts.hindawi.com/, according to the following timetable:

Manuscript Due	July 1, 2009
First Round of Reviews	October 1, 2009
Publication Date	January 1, 2010

Lead Guest Editor

Frank Ehlers, NATO Undersea Research Centre (NURC), Viale San Bartolomeo 400, 19126 La Spezia, Italy; frankehlers@ieee.org

Guest Editors

Warren Fox, BlueView Technologies, 2151 N. Northlake Way, Suite 101, Seattle, WA 98103, USA; warren.fox@blueview.com

Dirk Maiwald, ATLAS ELEKTRONIK GmbH, Sebaldsbrücker Heerstrasse 235, 28309 Bremen, Germany; dirk.maiwald@atlas-elektronik.com

Martin Ulmke, Department of Sensor Data and Information Fusion (SDF), German Defence Research Establishment (FGAN-FKIE), Neuenahrer Strasse 20, 53343 Wachtberg, Germany; ulmke@fgan.de

Gary Wood, Naval Systems Department DSTL, Winfrith Technology Centre, Dorchester Dorset DT2 8WX, UK; gwood@mail.dstl.gov.uk

Journal of Computer Systems, Networks, and Communications

Special Issue on WiMAX, LTE, and WiFi Interworking

Call for Papers

Although WiMAX, LTE, and WiFi provide wireless broadband connectivity, they have been optimized for different usage models: WiFi for very high-speed local area network connectivity and WiMAX, LTE for high-speed wireless cellular connectivity. By combining WiMAX, LTE, and WiFi technologies, service providers can offer better usability of the networks infrastructure and support for seamless mobility and roaming. The unique similarities between WiMAX, LTE, and WiFi networks that make the proposed synergy promising is these technologies are fully packet switching uses IP-based technologies to provide connection services to the Internet. This standards- and IP-based network approach provides compelling benefits to service providers to collaborate between these technologies.

This special issue is intended to foster state-of-the-art research in the area of WiMAX, WiBro, LTE, and WiFi networking, and the corresponding technical advances in the design and deployment of feasible network architectures and protocols, and to present novel results and solutions to solve various problems and challenges foreseen in WiMAX, LTE, and WiFi interworking. The special issue will cover the following topical areas but are not limited to them:

- WiMAX, WiBro, MobileFi, LTE, and WiFi communications systems
- Single/dual radio handover
- Network architecture alternatives for interworking and integration
- Heterogeneous wireless networks
- Seamless vertical handover and session continuity
- Multiradio coexistence and power management
- Authentication, authorization, and accounting
- Security issues
- Common charging and billing
- Quality of services (QoS)
- Interworking using IMS, SIP, MIH, VCC, and UMA
- IEEE802.11u, IEEE802.16g/j/m/h
- Scenarios and usage cases
- WiMAX,WiBro, LTE, and WiFi Interworking Testbed
- Hybrid wireless mesh network
- Applications, VOIP, video streaming, and so forth
- IP Mobile, roaming, and mobility management
- Core network architecture
- Fixed-mobile convergence (FMC)
- PHY, MAC, IP, and upper layers issues

Before submission authors should carefully read over the journal's Author Guidelines, which are located at http://www.hindawi.com/journals/jcsnc/guidelines.html. Prospective authors should submit an electronic copy of their complete manuscript through the journal Manuscript Tracking System at http://mts.hindawi.com/, according to the following timetable:

Manuscript Due	October 1, 2009
First Round of Reviews	January 1, 2010
Publication Date	April 1, 2010

Lead Guest Editor

Rashid A. Saeed, Telekom Malaysia R&D Sdn. Bhd. Lingkaran Teknokrat Timur, 63000 Cyberjaya, Selangor D.E., Malaysia; drrashid.saeed@tmrnd.com.my

Guest Editors

Ahmed A.M Hassan Mabrouk, Department of Computer Science, International Islamic University Malaysia, Kuala Lumpur, Malaysia; mabrouk@kict.iiu.edu.my

Amitava Mukherjee, IBM GBS India, Salt Lake, Calcutta 700 091, India; amitava.mukherjee@in.ibm.com

Francisco Falcone, Página principal de la Universidad Campus de Arrosadía 31006 Pamplona, Navarre, Spain; francisco.falcone@unavarra.es

K. Daniel Wong, Daniel Wireless LLC, Palo Alto, CA 94306, USA; daniel_wong@ieee.org

EURASIP Journal on Advances in Signal Processing

Special Issue on Microphone Array Speech Processing

Call for Papers

Significant knowledge about microphone arrays has been gained from years of intense research and product development. There have been numerous applications suggested, for example, from large arrays (on the order of >100 elements) for use in auditoriums to small arrays with only 2 or 3 elements for hearing aids and mobile telephones. Apart from that, array technology has been widely applied in the areas of speech recognition and more recently surveillance. Traditional techniques that have been used for microphone arrays include the fixed spatial filter as well as optimal and adaptive beamforming. These techniques model input or calibration signals as well as localization information for their design. Today contemporary techniques using blind signal separation (BSS) and time frequency masking techniques have attracted significant attraction. Those techniques are less reliant on array modeling and localization, but more on the statistical properties of speech signals such as sparseness, non-Gaussianity, nonstationarity, and so forth. The main advantage that multiple microphones add from a theoretical perspective is the spatial diversity, which is an effective tool to combat interference, reverberation, and noise when used according to the theoretical assumption. Combining spatial information with time-frequency information and perceptual cues will lead to innovative techniques and new methods, which will provide improved communication capabilities in challenging acoustic environments.

To further enhance current research and to promote new applications, this special issue aims to collect and present the latest research efforts in signal processing methods and algorithms for microphone arrays.

Topics of interest include, but are not limited to:

- Optimal and adaptive beamforming
- Blind signal extraction methods
- Multichannel dereverberation techniques
- Microphone array-assisted multichannel acoustic echo cancellation
- Spatial filtering techniques
- Sound source localization and tracking
- Psychoacoustically motivated procedures and algorithms such as perceptual cues, hearing thresholds, and spatial masking effects
- Distributed microphone networks
- Spherical array of microphones and Eigen/Modal beamforming

Before submission authors should carefully read over the journal's Author Guidelines, which are located at http://www.hindawi.com/journals/asp/guidelines.html. Prospective authors should submit an electronic copy of their complete manuscript through the journal Manuscript Tracking System at http://mts.hindawi.com/, according to the following timetable:

Manuscript Due	August 1, 2009
First Round of Reviews	November 1, 2009
Publication Date	February 1, 2010

Guest Editors

Sven Nordholm, Western Australian Telecommunications Research Institute (WATRI), Curtin University of Technology, Perth, WA 6009, Australia; sven@watri.org.au

Thushara Abhayapala, Department of Information Engineering, Research School of Information Sciences and Engineering, ANU College of Engineering and Computer Sciences, The Australian National University, Canberra, ACT 0200, Australia; thushara.abhayapala@anu.edu.au

Simon Doclo, NXP Semiconductors, Corporate I&T-Research, Interleuvenlaan 80, 3001 Leuven, Belgium; simon.doclo@nxp.com

Sharon Gannot, School of Engineering, Bar-Ilan University, 52900 Ramat-Gan, Israel; gannot@macs.biu.ac.il

Patrick Naylor, Department of Electrical and Electronic Engineering, Imperial College, London SW7 2AZ, UK; p.naylor@imperial.ac.uk

Ivan Tashev, Microsoft Research Redmond, One Microsoft Way, Redmond WA, 98052-6399, USA; ivantash@microsoft.com